Mechanisms controlling the intra-annual mesoscale variability of SST and SPM in the southern North Sea

Pietrzak, J.D.; de Boer, G.J.; Eleveld, M.A.

published in
Continental Shelf Research
2011

DOI (link to publisher)
10.1016/j.csr.2010.12.014

document version
Peer reviewed version

Mechanisms controlling the intra-annual mesoscale variability of SST and SPM in the southern North Sea

Pietrzak, J.D., Boer, G.J. de, Eleveld, M.A.

Continental Shelf Research, 31(6), 594-610

Mechanisms controlling the intra-annual mesoscale variability of SST and SPM in the southern North Sea

Julie D. Pietrzak [a,*], Gerben J. de Boer [a,c], Marieke A. Eleveld [b]

[a] Delft University of Technology (TU Delft), Section of Environmental Fluid Mechanics, P.O. Box 5048, 2600 GA Delft, The Netherlands

[b] Vrije Universiteit Amsterdam, Institute for Environmental Studies (VU-IVM), De Boelelaan 1087, 1081 HV Amsterdam, The Netherlands

[c] Deltares (former WL|Delft Hydraulics), P.O. Box 177, 2600 MH, Delft, The Netherlands

[*] Corresponding author. Tel.: +31 15 2781953; fax: +31 15 2784842.

E-mail addresses: J.D.Pietrzak@tudelft.nl (J.D. Pietrzak), g.j.deboer@tudelft.nl (G.J. de Boer), marieke.eleveld@vu.nl (M.A. Eleveld).

Research highlights

- Examination of SST and SPM images of the southern North Sea shows pronounced mesoscale variability.
- The Rhine ROFI, East-Anglia Plume and a seasonal thermal front dominate SST and SPM signals.
- Harmonic analysis highlights pronounced seasonal and spring–neap variability.
- Tides and waves control stratification and hence the visibility of near-surface SPM in the images.

This manuscript was published by Continental Shelf Research, © Elsevier

Always cite this paper as

Pietrzak, J.D., de Boer, G.J., Eleveld, M.A., 2011. Mechanisms controlling the intra-annual mesoscale variability of SST and SPM in the southern North Sea. Continental Shelf Research 31(6), 594-610. doi:10.1016/j.csr.2010.12.014

http://dx.doi.org/10.1016/j.csr.2010.12.014

Abstract

Thermal and optical remote sensing data were used to investigate the spatial and temporal distribution .of sea surface temperature (SST) and of suspended particulate matter (SPM) in the southern North Sea. Monthly SST composites showed pronounced seasonal warming of the southern North Sea and delineated the English coastal and continental coastal waters. The East-Anglia Plume is the dominant feature of the English coastal waters in the winter and autumn SPM composites, and the Rhine region of .freshwater influence (ROFI), including the Flemish Banks, is the dominant feature of the continental .waters. These mesoscale spatial structures are also influenced by the evolution of fronts, such as the .seasonal front separating well-mixed water in the southern Bight, from the seasonally stratified central .North Sea waters. A harmonic analysis of the SST and SPM images showed pronounced seasonal .variability, as well as spring–neap variations in the level of tidal mixing in the East Anglia Plume, the .Rhine ROFI and central North Sea. The harmonic analysis indicates the important role played by the .local meteorology and tides in governing the SST and near-surface SPM concentrations in the southern .North Sea. In the summer, thermal stratification affects the visibility of SPM to satellite sensors in the .waters to the north of the Flamborough and Frisian Fronts. Haline stratification plays an important role .in the visibility of SPM in the Rhine ROFI throughout the year. When stratified, both regions typically .exhibit low surface SPM values. A numerical model study, together with the harmonic analysis, .highlights the importance of tides and waves in controlling the stratification in the southern North Sea .and hence the visibility of SPM.

Keywords: Remote sensing, NOAA AVHRR Sea surface temperature, SeaWiFS suspended particulate matter, Shelf sea stratification, Wind and tidal mixing, Turbidity

1. Introduction

The southern North Sea (Fig. 1) is a dynamic region dominated by two large regions of freshwater influence (ROFIs); the Rhine ROFI (Simpson et al., 1993; McCandliss et al., 2002; de Boer et al., 2006) and the East Anglia Plume (McCave, 1987), as well as a seasonal tidal mixing front that extends across the southern North Sea in the summer (Eisma and Kalf, 1987; Hill et al., 1993). Tidal, meteorological and buoyancy driven residual currents result in a strong cyclonic circulation in the central North Sea, which turns into an eastward flow at the location of the East Anglia Plume (Prandle, 1978; Prandle et al., 1993). This flow is enhanced by a predominant northward flow through the Dover Straits and southern Bight. As with the Rhine ROFI, the Tees, Humber and Wash act as classic river plumes. Under the influence of the Coriolis force their fresher waters deflect to the right upon exiting their respective river mouths. In contrast, the residual circulation causes the Thames outflow to deflect to the left. It then becomes part of the offshore deflected buoyant coastal waters of the East Anglia Plume that cross the southern North Sea at about 53° latitude (Holt and James, 1999). The East Anglia Plume is known to be a zone of high turbidity, extending along the East Anglia coast, over the Norfolk Banks, and across the southern Bight towards the German Bight (Dyer and Moffat, 1998). The Rhine ROFI also controls the northwards transport of SPM in the southern North Sea (Dronkers et al., 1990; Visser et al., 1991). Using the Simpson and Hunter (1974) parameter, Pingree and Griffiths (1978) predicted that the

seasonal tidal mixing front should also form at the approximate location of the East Anglia Plume, at Flamborough Head and the Frisian Front. It separates well-mixed water in the southern Bight, from the seasonally stratified central North Sea waters. It controls not only the evolution of jet like along front flows and primary productivity (Hill et al., 1993), but also the evolution of deep jets, associated with the presence of the seasonal thermocline (Brown et al., 1999; Hill et al., 2008).

These ROFIs and fronts dominate the southern North Sea, influencing the transport of freshwater, sediment, biota and pollutants. Hence it is important to understand the factors influencing the spatial and temporal variability of these mesoscale structures. Advanced very high resolution radiometer (AVHRR) and other SST sensors, as well as ocean colour sensors (SeaWiFS, MODIS and MERIS), offer the potential to observe the physical oceanographic characteristics of shelf seas such as this. The aim of this paper is to explain the intra-annual variability in remotely sensed sea surface temperature (SST) and suspended particulate matter (SPM) patterns in the southern North Sea observed in one example year, 1998. As part of this, we consider the forcing mechanisms and oceanographic characteristics of this region, and the assumptions and limitations associated with SST and SPM remote sensing (RS) products.

The methods are described in Section 2. Every AVHRR SST and SeaWiFS SPM image available for 1998 was examined. We build upon previous studies in which SST images were used to assess the offshore extent of the Rhine ROFI (de Kok et al., 2001; Arentz, 2005; de Boer et al., 2009) and extend their methods to the southern North Sea. We use the algorithms developed by van der Woerd and Pasterkamp (2004) and Eleveld et al. (2004, 2006, 2008) to calculate near-surface SPM concentrations for these optically complex southern North Sea waters (referred to as Case 2 waters by Morel and Prieur, 1977). In order to characterise the intra-annual temporal and spatial variability, an analysis of meteorological and run-off data, together with both a harmonic analysis of the remote sensing data and numerical simulations of tides and waves, has been carried out. These ancillary data are used to help interpret the SST and SPM satellite images. Sections 3.1 and 3.2 present the monthly evolution of the spatial distributions of both SST and SPM. Here, we also consider the role of buoyancy forcing, which stratifies the water column versus tides, winds and waves, which mix the water column. Sections 3.3 and 3.4 present the results of the harmonic analyses and quantify the seasonal and spring–neap variability. In Section 3.5 we consider the role of stratification on the distribution of SST and SPM, and its role on the visibility of SPM at the surface. Finally conclusions are presented in Section 4.

2. Methods

2.1. SST processing details

Processed SST data from the polar orbiting NOAA advanced very high resolution radiometer (AVHRR) satellites were obtained from the Royal Dutch Meteorological Institute (KNMI), who operate a high resolution picture transmission (HRPT) receiving station and provided 1.1 km local area coverage (LAC) resolution. The data were supplied as readily processed Level 2 (L2) data (Roozekrans and Prangsma, 1992). The SST L2 data were binned on a rectangular polar stereographic projection. After stereographic projection the data were manually geo-referenced (shifted) using distinctive Ground Control Points on the Dutch coastline. The vegetation index image (using channels 1 and 2) was used for this, as in this image the coastline is the most visible. After this manual correction the accuracy is ~1–2

km. However, due to the fact that the data were not geo-referenced until after projection, the images are slightly distorted and cannot always be shifted to fit the whole coastline. Images on which the Dutch coastline was not visible at all could not be geo-referenced and were discarded by KNMI. The SST data set therefore show a strong bias towards unclouded pixels in the Rhine ROFI region (Fig. 2). Cloud identification masks were also created using visible and infrared channels with a series of spectral gradient, difference and threshold tests (Saunders and Kriebe, 1988) Sometimes, as a side-effect, the strong gradients present on the margins of a stratified plume subject to solar heating were flagged off as clouds.

2.2. SPM processing details

The SeaWiFS sensor registers radiance in the optical and near infrared wavelengths. The SeaWiFS data have been recorded at 1.1 km LAC resolution by the NERC satellite receiving station at Dundee University, UK. SeaWiFS data (Raw level 1A HRPT data) were obtained from NASA. Following van der Woerd and Pasterkamp (2004), the 1998 data were atmospherically corrected with SeaDAS 4.0 (see NASA http://oceancolor.gsfs.nasa.gov/seadas) using the algorithms developed by MUMM for turbid Case 2 waters (Ruddick et al., 2000). Although this algorithm requires manual calibration per image per small region (order 200 km), it was decided to apply default coefficients throughout the year (α=1.72, γ=1.0, ε78=1.05). Although we were aware that it might cause small inaccuracies, while α has a rather constant default value, the slope of the aerosol dominated part of the reflectance, ε78 can vary between 0.96 and 1.15 (Eleveld practical experience; Ruddick et al., 2000). The resulting variability in radiance (nLw555) has been quantified in Table 1 of Ruddick et al. (2000). However, in practise it is only likely to become important in clear waters with a hazy atmosphere. Subsequent propagation to variability in SPM (Eleveld et al., 2008) will be averaged out in the monthly averages that are presented here (Pasterkamp et al., 2003). SPM concentration was determined from the POWERS algorithm (Pasterkamp et al., 2005; Eleveld et al., 2004, 2006, 2008), using R0- obtained from nLw as described in Morel and Gentili (1996) with Q0 set to π. Next the SeaWiFS data were cropped and gridded to exactly the same rectangular polar stereographic grid as the SST data, allowing for pixel by pixel comparison. Further details on RS data levels, data acquisition and data processing can be found in Arentz (2005).

2.3. Spatial and temporal availability of satellite data

Both SST and SPM images provide a spatial resolution of approximately 1 km^2. The maximum data availability of a NOAA satellite is 2 images per day. During most of 1998 two satellites were in operation (NOAA12 and 14), in August a third joined (NOAA15). This gives a temporal resolution of up to 6 images per day. The maximum data availability of SeaWiFS is 1–2 images per day. Due to cloud cover not all satellite passes yield usable images, hence only 167 SST images and 163 SPM images with a cloud-free Dutch coastal zone were obtained. The clustering of the images in time is evident in Fig. 2 as well as the spatial distribution of the number of available images used to make the annual SST and SPM composites. It should be noted that the winter SPM composites are based on only a few images (Fig. 2). Due to the extensive cloud cover in this season only a partial composite is available for November and no composite is available for December 1998. Fig. 2 also shows that the annual mean SST is warmer in the

southern North Sea than the deeper northern regions. The highest SPM levels were found near the Humber estuary and in the Greater Thames Estuary at the head of the East Anglia Plume and near the shallow Flemish Banks. The annual standard deviation is highest within the region of the Flemish Banks, the Rhine ROFI and the East Anglia Plume and Frisian Front.

The Internal Rossby Radius of Deformation (RoI) is taken as the division between baroclinic mesoscale and sub-mesoscale spatial scales and is typically of the order 10 km in the study area. The availability of data at 1–2 images per day, together with the 1 km^2 spatial resolution of SST and ocean colour satellite data, allows us to investigate the mesoscale oceanographic structures associated with these ROFIs and fronts in the southern North Sea, including the temporal and spatial scales associated with baroclinic instability.

2.4. Meteorological data

The meteorological data consist of wind from K13 and irradiance data from Den Helder, and river discharge data from the Rhine-Meuse system. K13 is a station centrally located within the southern North Sea. A comparison was carried out between K13 and a number of Dutch stations (not shown here) and very good agreement was found between the wind speed and direction at the stations. The temperature, discharge and solar radiation data were made available on internet by the Dutch ministry of public works (Rijkswaterstaat, the Netherlands), the wind data by the Royal Dutch Met Office (KNMI).

2.5. Tide and wave simulations

The flow modelling system Delft3D-FLOW (Stelling and Van Kester, 1994) and wave modelling system SWAN (Booij et al., 1999) were setup to simulate tides and waves in the southern and central North Sea. The domain is presented in Fig. 1. Barotropic simulations were carried out with 10 sigma layers in the vertical. The models have a grid size of about 2 km in the continental coastal zone from Belgium to the German Bight. Towards the open boundaries, across the central North Sea, from the tip of Denmark to Scotland, the resolution decreases to about 25 km. A detailed description of the flow model setup and its validation can be found in Gerritsen et al. (2000, 2001) and Roelvink et al. (2001).

First a tidal simulation was run as a reference case. For this simulation February 1, 1998, was chosen, as it was approximately halfway between spring and neap tides. The maximum bed shear stresses were computed during one semi-diurnal tidal cycle. This simulation was used as the reference case with which to calculate h/u^3 contours due to the tides, where h is the depth and u is the amplitude of the tidal velocity. Then the barotropic tidal setup was run, but this time it employed a two-way coupling with an hourly wave simulation, using SWAN. Two wave scenarios were considered using typical wind speeds and directions (Holt and James, 1999; Fettweis and Van den Eynde, 2003). The model was run with constant 10 m s^{-1} winds from the SW and NW; the corresponding maximum wave induced bed stresses were calculated following Swart (1974).

The deposition and erosion of sediment is related to a critical value of the bed shear stress. Mud is deposited when the critical bed shear stress is below 0.1–0.2 N m^{-2} and it is typically eroded if it is above

0.4–0.5 N m^{-2}. Holt and James (1999) used a value of τ_{ero}=0.41 N m^{-2}, where τ_{ero} is the critical stress for resuspension. In their Fig. 1, they plotted contours of τ_{ero}=50% showing the fraction of the spring–neap tide cycle during which the bed stress, t, based only on the tidal currents is above the critical value, τ_{ero}, for resuspension, $\tau > \tau_{ero}$. They found this characterised the regions where the tides alone were effective in resuspending bed material. Here we plot contours of bed shear stress. The tidal model results were also used to calculate the position of the lines that delineate the seasonal stratification according to the Simpson–Hunter criterion using the same definition as Pingree and Griffiths (1978), where the velocity amplitude *u* was determined by applying the Fourier analysis for the M2 component that was performed during the simulation using information from all time steps.

2.6. Harmonic analysis

A harmonic analysis (e.g. von Storch and Zwiers, 1999) of the SST and SPM remote sensing images was carried out for each pixel separately from a set of remote sensing images. The following equation was used when performing the analysis:

$$\psi(x,y,t) = A_0(x,y) + \sum_{i=1}^{i=n} A_i(x,y)\cos(\omega_i t + \varphi_i(x,y)) + \varepsilon(x,y,t) \quad (1)$$

where $\psi(x,y,t)$ represents either the SST or the SPM images, t is time, x and y are the spatial co-ordinates of each pixel in a Cartesian co-ordinate system, $A_0(x,y)$ represents the mean value at each pixel and $A_i(x,y)$ represents the amplitude of harmonic signals where i=1 the seasonal (annual) cycle, i=2 the spring– neap cycle (the fortnightly variability) and ω is the frequency and $\varphi_i(x,y)$ is the phase in radians and $\varepsilon(x,y,t)$ is the error after the least squares fit. The harmonic analysis was carried out on all the images. A harmonic analysis was carried out for all 1998 SST (>160) and SPM (>160) images. The bathymetry contours and the location of the calculated h/u^3 contours were plotted in all figures and compared to the seasonal thermal front as described in Pingree and Griffiths (1978).

3. Results and discussion

3.1. Monthly sea surface temperature variability

Fig. 3 illustrates the seasonal cycle of warming and cooling in the southern North Sea. The bands of colder coastal waters in the winter, and the warmer coastal waters in the summer, are well defined features of the SST imagery, as well as the in situ data (Fig. 4a). They delineate the English and Continental coastal waters from the warmer winter and cooler summer Channel waters. The Rhine ROFI and East Anglia Plume are pronounced features of the images. The three hydrographic regions correspond with the description in Otto et al. (1990), although they are not water masses; SST quickly responds to changes in meteorological forcing. The seasonal warming and cooling of the southern North Sea observed in Fig. 3 compares well with the increasing and decreasing solar irradiation throughout the year (Fig. 4c). The seasonal cycle of irradiation is well defined, with minima in January and December and a maximum in the summer. The temperatures at 1 m below the surface follow the changes in solar irradiation. Note

also the big peak from early to mid-May, with the largest values centred at May 12–14, as well as the rapid increase in surface temperature from mid-April to mid-May.

Fig. 5 shows that the winds were predominantly from the SW and between 10 and 20 m s^{-1} in the winter months. Fig. 6a shows the maximum bed shear stresses simulated for one semi-diurnal tidal cycle. It reflects the propagation of the semi-diurnal tidal wave around the southern North Sea and indicates regions where there is likely to be higher mixing. On this date the tide is approximately mid-way between neap and spring tides. Hence there will be a spring–neap modulation of the magnitude of the bed stresses about these values. Fig. 6b shows the corresponding maximum wave stresses modelled using a constant 10 m s^{-1} wind from the SW. The wave induced bed stresses add a time variable shear stress component to the tidal distribution and are of a comparable magnitude to the tidal stresses. Both the tide and waves will mix the water column in the southern North Sea.

The locations of the East Anglia Plume and English coastal waters are most discernible in the winter and autumn months of 1998, from January to March 1998 and again from September onwards (Fig. 3). In the winter and autumn the Rhine ROFI exhibits a clear upstream bulge as well as a downstream plume. The bulge region extends from the mouth of the Rotterdam Waterway southwards along the Belgium coast and includes the Flemish Banks. The downstream part of the ROFI extends from the mouth, northwards to the Wadden Sea and beyond. The transition from a cold to warm Rhine ROFI takes place in March and from a warm to cold plume takes place in September. This is also observed in the annual SST data presented in Fig. 4a for stations along the Dutch coast. The Rhine River discharge is highly variable with the largest discharges in the winter and autumn, reaching a minimum in the summer months. November was marked by an exceptional peak of 7164 m^3 s^{-1} on the 6th, which only diminished to 3000 m^3 s^{-1} after the 21st (Fig. 4b). In the southern ROFI region, near the Flemish Banks, the SST images (Fig. 3) also indicate the presence of warmer/colder river waters to the south of the Rotterdam Waterway. In accordance with the findings of Lacroix et al. (2004) the warmer/colder Rhine ROFI waters recorded off the Belgium coast likely correspond to well-mixed waters at this upstream location of the Rhine ROFI. They showed that most of the fresher water in the Belgium coastal zone originates from the Rhine outflow and that the water column at this upstream location is always well-mixed; stratification of the order 0.2 PSU and 1 °C is only occasionally observed under calm summer conditions, note the large tidal stresses at this location in Fig. 6a. Visser et al. (1994) and Simpson et al. (1993) found that under typical discharge conditions and spring tides the downstream region of the Rhine ROFI is mixed over the vertical, whereas on neap tides it is stratified.

The East Anglia Plume is evident as the northern boundary of the warmer Channel waters in winter (Fig. 3). In the summer, SST does not appear to delineate the East Anglia Plume as clearly. In contrast to the Rhine ROFI, the waters of the East Anglia Plume are known to be well-mixed. This is because the buoyancy inputs from the river discharges are much less than those of the Rhine and the tidal stresses are much larger along the British coast (Fig. 6a). However, there is some evidence from Baars et al. (2003) that the East Anglia Plume becomes weakly stratified in the summer. This is likely associated with the decreasing wind and wave stresses in the summer (Figs. 5 and 6b), as well as tidal and wind driven straining.

The Simpson–Hunter parameter indicates that most of the southern North Sea (S=1) should be well-mixed by the tide (Fig. 6). It is evident that the buoyancy inputs from the Rhine (Fig. 4b) are great

enough to cause stratification (albeit modulated by the tides) throughout the year along the Dutch coast. Wind (Fig. 5) and waves (Fig. 6b) will also make a significant contribution to mixing of the Rhine ROFI in winter. Large regions of the southern North Sea have warmed by the summer months, particularly June and July, making it more difficult to distinguish the ROFIs and fronts in the monthly composites.

3.2. Monthly suspended particulate matter variability

Fig. 7 illustrates a distinct seasonal cycle of SPM with increased surface concentrations of SPM in the autumn and winter, and diminished values in the late spring and summer. The winter months are characterised by high SPM concentrations along the Belgium, Dutch, German and UK coasts, particularly at the locations of the Rhine ROFI, and the East Anglia Plume. In these regions SPM is mixed throughout the entire water column. The seasonal changes in near-surface SPM concentration are in agreement with previous studies, using cruise data (Eisma, 1981, 1993; Eisma and Kalf, 1987; North Sea Task Force, 1993; Dyer and Moffat, 1998), surface reflectance (Holligan et al., 1989; van Raaphorst et al., 1998), in situ optical techniques (Postma, 1961; Otto, 1966, 1967; Visser, 1970) and SPM Atlases (Pasterkamp and van Drunen, 2002; Pasterkamp et al., 2003). The latter authors found the highest concentrations in January and February of 2000 and 2001, whereas in Fig. 7, the East Anglia Plume is most pronounced in March 1998. In the late spring and summer SPM drops to minimal values. This appears to coincide with the decreased storm activity, lower winds and waves and hence less resuspension from the seabed (Figs. 5 and 6b). It also coincides with increased summer stratification.

Fig. 6a indicates where tidal deposition and resuspension of fine grained sediments (predominantly mud and silt) might occur. If one compares Figs. 7 and 6a, the regions where the tidal shear stresses alone are large enough to resuspend mud are evident. These regions, to the south of the τ_{ero}=2.0 N m^{-2} contour, are consistent with the location of the Holt and James (1999) τ_{ero}=50% contour. They are all located in the southern North Sea (and English Channel) and extend northwards along the Lincolnshire and East Anglia coasts. These are also the regions where the tides are more likely to keep the water column well-mixed throughout the year. High surface SPM to the south of τ_{ero}=2.0 N m^{-2} is visible in the shallow regions (order 15–25 m), near the Flemish Banks and near the mouth of the Thames, the Wash and offshore from Holderness. In these regions any deposited material will quickly resuspend. This suggests that there must be a local transitory source of mud present at the bed in the shallower regions, mostly kaolinitic clay minerals in the East Anglia Plume (Eisma, 1981; Irion and Z¨ ollmer, 1998). In regions where τ_{ero}=0.5 N m^{-2} significant resuspension by tides alone is unlikely. In Fig. 7 low surface SPM concentrations tend to be recorded in these regions. The wave induced bed stresses add a time variable shear stress component to the mean tidal distribution (Fig. 6b). Fig. 8a shows a significant increase in the bed stresses due to waves, along the Dutch coast, near the mouth of the Thames and near the Dogger Bank. However, both the Dogger Bank and the region defined as Channel waters by Otto et al. (1990) are low in surface SPM, the former region is a relatively uniform sandy area and coarser materials also populate the Channel bed (Lafite et al., 2000). Even if the bed stresses are great enough to resuspend bed material there has to be a supply of fine sediment (mud/silt) available at the bed for resuspension, if it is to be recorded by surface sensors.

A turbidity maximum is evident near the shallow Flemish Banks in all of the images. It is most pronounced in winter and shows a significant reduction in the summer. This suggests that tides keep the

water column well-mixed and keep SPM in suspension even in summer, but that the combined tide and wave stresses (Fig. 8a) are responsible for the higher SPM values in the winter. The turbidity maximum is thought to be related to a local eddy in the residual recirculation (Nihoul and Hecq, 1984; van Alphen, 1990), or to convergence associated with decreasing residual currents and import of SPM through the Strait of Dover (Fettweis and Van den Eynde, 2003). A local SPM minimum, about 30 km off the Dutch coast, is also recorded in the winter images, in agreement with Visser et al. (1991) and Suijlen and Duin (2001, 2002).

The regions with τ_{ero} between 0.5 and 2.0 N m^{-2} will likely be subject to wind and wave driven resuspension. If one compares Figs. 6 and 8a it is evident that the τ_{ero}=2.0 N m^{-2} contour is now located farther offshore and extends across the southern North Sea from the Norfolk Banks to the Frisian Front. This is at the approximate location of the offshore extension of the East Anglia Plume at ~54°N between 3 and 5°E. As the wave stresses increase in winter (Figs. 5 and 6b) bed material is more likely to be resuspended in these months and there is a source of fine sediment at the bed (Fig. 8b). Here the combined τ_{ero} lies between 1.0 and 2.0 N m^{-2} indicating that resuspension by wind and wave driven stresses may be responsible for the visibility of the plume at this offshore location. The regions north and south of the East Anglia Plume do not show resuspension during storms (Fig. 7). This is most likely because there is no source of mud at the bed in the shallower waters to the south, whereas to the north of the plume it is deeper and the combined τ_{ero} <0.5 N m^{-2}. The Oyster Grounds (Fig. 8b) are known to be a major region for the deposition of fine sediment (Eisma and Kalf, 1987).

Higher SPM concentrations are recorded in the shallow waters near the mouth of the Thames, the East-Anglia and Lincolnshire coasts, and within the East Anglia Plume from January to April and September to October 1998 (Fig. 7), in agreement with Pleskachevsky et al. (2005). The majority of the SPM transport occurs in winter when the erosion of the cliffs along the English coasts is the greatest. The SPM maximum, within the East Anglia Plume, coincides with the location of the cyclonic wind driven residual circulation that is known to be most pronounced during periods of SW winds (Fig. 5). Holt and James (1999) show that sediment eroded at Holderness in October is advected southwards to the Norfolk coast by mid-November, and forms a welldefined offshore sediment plume by mid-February/March. Their simulations, as well as North Sea Project data, also found the most intense plume in March 1989 and that deposition typically occurs along the 40 m depth contour. The area with the greatest percent (40–50%) of mud deposits in Fig. 8b lies along the 40 m contour and coincides with the offshore location of the East Anglia Plume. Time series of SPM (Holt and James, 1999) show that SPM is only measured in the water column in a discrete series of events associated with increased wind activity. They showed that the sudden increase of SPM throughout the entire water column was consistent with well-mixed conditions and resuspension of bed material. They also found that once resuspended, SPM remains in suspension in the water column for about seven days, and that during summer virtually all SPM settles out. The bed composition will therefore most likely mimic the type of sediment in the water column. In the summer, the bed can contain fine grained sediment smaller than 70 μm dispersed in the sand (Eisma, 1981), but it is not resuspended due to the absence of sufficient wave action (Fig. 6b). The locations where the maximum tidal stresses are below 2 N m^{-2} are likely to experience periods of erosion during stormy conditions, followed by deposition during periods of calm weather.

3.3. Harmonics in the 1998 SST and SPM data

Figs. 9 and 10 show the spatial variation of the amplitude of the seasonal cycle and spring–neap cycle, respectively, for (a) SST and (b) SPM in 1998. The largest amplitude variations in the seasonal temperature cycle occur in the shallow regions (Fig. 9a). The corresponding phase results (not shown) show an increasing phase delay with depth, with maximum seasonal temperatures occurring 1 month later in the deeper waters than in shallow waters. This is in agreement with the variability observed in the monthly remote sensing (Fig. 3) and station data (Fig. 4). There is also a distinct spatial distribution in the SPM; the largest amplitude variations are at the location of the East Anglia Plume and in the region of the continental coastal waters, in agreement with Fig. 7. The large amplitude variations in SPM occur at the same location as the large seasonal temperature variations, giving a qualitative correlation between SST and SPM in the shallow regions of the English coastal waters and the continental coastal waters. The shallow waters and large tidal and wave driven shear stresses (Fig. 6) allow a rapid response to surface heating and cooling; they also allow the waters to become well-mixed and for sediment to be resuspended throughout the water column.

In addition, a band with large variations in the amplitude of the seasonal SPM harmonic is found to the east of the Norfolk Banks in depths of about 20–30 m. This band stretches across the southern North Sea towards the German coast. Its location correlates with the region affected by the large tidal stresses, and increased wave induced stresses in the winter (Fig. 8a). Additionally, the East Anglia Plume is located at about the same place as the seasonal maximum in the amplitude of the offshore temperature in Fig. 9a, with the maximum in SST slightly more to the north. Fig. 9a shows seasonal maximum amplitudes of 5 °C, whereas the waters over the Norfolk Banks and the Channel waters have seasonal amplitudes of 4 °C.

The monthly means (Fig. 3) indicate that this is the northern limit of the warmer Channel waters in winter. During 1998 the winter images clearly delineate the colder turbid English coastal and Continental river waters from the warmer Channel waters (Figs. 3 and 7). The three hydrographic regions come close together just north of Texel, at the western edge of the Wadden Sea. Here the Channel waters narrow into the long Frisian Front filament separating the colder, more turbid continental coastal waters from the colder, more turbid East Anglia Plume to the north of it. This filament is most clearly visible in January as a narrow band of water with higher temperature and lower turbidity that extends north-eastward.

A distinct spring–neap variation in the amplitude of both SST and SPM (Fig. 10) indicates that they respond to the variation in tidal forcing through the spring–neap cycle and hence to the amount of energy available for mixing and for bed-resuspension (Fig. 6). The spring–neap SPM signal is similar to the seasonal signal, with the largest variations in the shallow coastal waters and offshore at the location of the East Anglia Plume. However, the variability in the amplitude of the spring–neap SST signal is completely different; the largest amplitude in the signal is found in the central North Sea waters, north of the approximate location of the seasonal tidal mixing front, the h/u^3 contours in Fig. 10. Moreover there is a distinct band of maximum SST amplitude variation in the Flemish coastal waters, near the Thames mouth and in the downstream region of the Rhine ROFI, while a region exhibiting only small amplitude variations during the spring– neap tidal cycle is found near the mouth of the Rhine ROFI. The bulge region in the immediate vicinity of the mouth tends to remain stratified even on spring tides (de Nijs et

al., 2011) and there is no significant spring–neap modulation. The Flemish coastal waters and the waters near the mouth of the Thames are known to be well-mixed. The spring–neap SST signal at these locations indicates that variation in the level of tidal energy available for mixing impacts the SST and therefore the whole water column. While both regions are well-mixed vertically, they exhibit along and cross-plume density variations and hence are subject to tidal straining (Simpson et al., 1993). It appears that this is the mechanism responsible for the visibility of these regions in the spring–neap SST harmonic. In contrast, the downstream region of the Rhine ROFI typically switches from a well-mixed state on springs to stratified on neaps (Souza and Simpson, 1997). The amplitude in the spring–neap signal observed here defines the offshore extent of the Rhine ROFI.

3.4. The East Anglia Plume and Rhine ROFI

The East Anglia Plume was named, after the distinct zone of high turbidity across the southern North Sea, as highlighted by the pronounced SPM maximum in the annual harmonic in Fig. 9b. The region of the East Anglia Plume from the English coast, to the south of the seasonal pycnocline, is always well-mixed. Therefore the demarcation of the East Anglia Plume by the SST harmonic (Fig. 9a) indicates the offshore extent of the freshwater plume too. The East Anglia Plume appears to be defined by both a buoyant plume, as well as a sediment plume, in agreement with recent cruise data (Baars et al., 2003). The buoyant plume lies somewhat to the north of the sediment plume, in agreement with their salinity and turbidity data. They found the buoyant plume is normally situated to the north of the silt plume due to the dominant SW winds. However, they found their relative positions could change, and that due to NW winds the freshwater plume could be located to the south of the silt plume. In the summer months the offshore location of the East Anglia Plume coincides with that of the more prominent Frisian Front.

Whenever the monthly composites record a high SPM value within the East Anglia Plume, they also record high values within the Rhine ROFI (including the Flemish Banks) and vice versa (Fig. 7). The greater wind speeds during this time of year and greater percentage of winds from the SW (Fig. 5) appear to coincide with the increased resuspension of sediment in these regions in the winter months. This is in agreement with Suijlen and Duin (2001, 2002) who used 20 years of surface SPM samples to compose maps of average SPM in the northern Rhine ROFI. A separate map based only on the data recorded after storms shows a sudden increase of SPM over the entire coastal zone. This can only be explained by local resuspension of sediment and not by advection from the sources in the southern ROFI, such as the Flemish Banks. It should be noted that during storms the Rhine ROFI is known to be well-mixed (Simpson et al., 1993).

Low SPM values coincide with decreased wind and wave activity (Figs. 5 and 6) and decreased erosion and/or resuspension events allowing SPM to settle, in agreement with the mud deposits in Fig. 8b. Souza et al. (2007) found that an increase in net deposition appears to correlate with decreased wind stress, and the decreased storm activity in the region of the seasonal thermal front. The results presented in Fig. 7 are also consistent with the results of Fettweis and Van den Eynde (2003) recorded in Belgium coastal waters. They found SPM concentrations to be 1.2 times higher in winter and 0.8 times lower in summer than in spring and autumn. The fact that the Rhine ROFI behaves in a similar manner to the East Anglia Plume leads one to suspect that there is a similar process governing the visibility of the winter SPM high and the summer SPM low. The waters near the Flemish Banks are also known to be well-

mixed throughout the year (Lee, 1980; Ruddick et al., 2000; Lacroix et al., 2004) and consequently SPM can be recorded by surface sensors.

The upstream (well-mixed) bulge region of the Rhine ROFI, near Zeebrugge, acts as a marine source of SPM for the downstream coastal current, whereas the Rhine River acts as a fluvial supply of sediment. The subsequent transport of SPM within the downstream part of the Rhine ROFI appears to depend on the state of the downstream plume. If it is a well mixed plume, then a band of SPM stretches from the Flemish Banks, over 100 km northwards, towards the Wadden Sea. In this case, the width of this band of SPM should be the same width as that recorded by the SST images. In contrast if the plume is stratified, the surface waters of the Rhine ROFI will contain almost no SPM, as it remains trapped beneath the pycnocline. This has indeed been observed by Joordens et al. (2001). In cross shore transects they show that matter tends to stay trapped below the pycnocline in the Rhine ROFI. However, this will apply, except for a narrow near shore band where upwelling of SPM can occur due to tidal straining (de Boer et al., 2009), and in the shallow near shore environment (< 7 m) where spring tides can enhance erosion and keep SPM in suspension.

It is interesting that the amplitudes of the spring–neap harmonic of SST (Fig. 10a) and SPM (Fig. 10b) show just this pattern of SST and SPM. That is, a broad area delineated by a large amplitude response in SST, but a narrow coastal region delineated by a larger amplitude SPM response. However, note that the offshore position of the ROFI appears to be delineated by the somewhat larger amplitude of the SPM response recorded along the edge of the ROFI, along the 20 m depth contour. This coincides with the approximate offshore location of the ROFI as defined by Fig. 10b. Hence the spring–neap variabilities of SST and SPM appear to allow us to delineate the approximate location of the Rhine ROFI. SST also defines a broad offshore plume, the cold plume of water visible in the winter months, and the warm plume visible in particular in May, in Fig. 3. Furthermore, this suggests that the downstream region of the Rhine ROFI is typically stratified during 1998, both in the winter months with large river discharges and in May with large heat fluxes. The annual harmonic of SST and SPM (Fig. 9) also appears to define the mean position of the Rhine ROFI.

A visual analysis of all of the individual images did not show any signs of significant baroclinic instability in 1998. The only instability-like features were observed along the Rhine ROFI in February 1998 (Arentz, 2005). However, they are most likely due to pulsed river discharge as discussed by de Ruijter et al. (1992). Friction (Fig. 8c) and the spring–neap (Fig. 10a) switching of the stratification likely preclude the development of baroclinic instabilities.

3.5. Effect of stratification on the visibility of SPM to ocean colour sensors

One of the main limitations with using remote sensing images arises because stratification affects surface optical properties. Indeed, both theoretical studies (Geyer, 1993) and a recent analysis of SPM data collected in the Rotterdam Waterway (de Nijs et al., 2010) showed that stratification leads to the shut down of turbulence at the pycnocline, causing any surface SPM in the waters above the pycnocline to settle out. Consequently, stratification has a large impact on our ability to measure SPM concentrations with surface sensors. One will only record a surface SPM signature, if the water column is well-mixed.

Moreover, if the water column is stratified, a low surface SPM concentration does not allow one to conclude that there is no sub-surface transport of SPM (Eleveld et al., 2008).

Numerical studies (Holt and James, 1999; Souza et al., 2007) have demonstrated that the seasonal thermal structure in the North Sea has a marked effect on the seasonal cycle of SPM. Souza et al. (2007) showed that when well-mixed, the bottom and surface boundary layers merge and there is enough turbulence to keep the SPM in suspension. Notably, when the water column is stratified the reduction in turbulence near the pycnocline causes a separation of the two boundary layers. Consequently while turbulent kinetic energy supplied by the tides can cause the resuspension of SPM, it is trapped in the bottom boundary layer. Due to the pycnocline, higher values of SPM are therefore concentrated near the bed. The tides can then resuspend sediment and distribute it throughout the lower layer of the water column, while above the pycnocline there is almost no SPM. A similar process occurs in the Rhine ROFI when it is stratified (Joordens et al., 2001; Wild-Allen et al., 2002). Their in situ observations showed that SPM can be resuspended by the tides, but that it is trapped below the pycnocline. They found that there can be a substantial sub-surface transport of SPM when the Rhine ROFI is stratified. Consequently it will not be visible at the sea surface.

The visibility of SPM to surface sensors in the southern North Sea is summarised in Fig. 11. The East Anglia Plume exhibits high surface SPM signals over a wide region during the well-mixed winter period (the bottom left and centre panels), when both sediment availability and resuspension events are prevalent. However, during the stratified summer season the central North Sea shows a low SPM signature over a narrow region (the top right panels). The low SPM values are due to limited resuspension events, in combination with the smaller sediment availability. The narrow surface signature is due to the trapping of SPM below the summer pycnocline (upper left panels). This is in agreement with Souza et al.'s (2007) summer picture of decreased surface SPM due to increased stratification, as well as a decrease in the supply of SPM in the summer months in the East Anglia Plume, caused by the decrease in erosion of the Holderness cliffs.

In the Rhine ROFI similar states can be distinguished, albeit with a different time scale. The Rhine ROFI is well-mixed during periods with high-mixing such as spring tides and storms (the upper right panel). During these periods high SPM values can be observed over the full width of the ROFI. The Rhine ROFI exhibits haline stratification during neap tides with low energy winds. During these periods SPM is trapped below the pycnocline, therefore SPM is not visible in the surface layer (middle right panel), as supported by de Nijs et al. (2010, 2011). An exception to this stratified case occurs for high river discharge events with high SPM loads shown in the lower right panel. During the winter the central North Sea is well-mixed such that no SPM can be hidden below the pycnocline. In addition, high SPM fluxes occur due to the high supply of sediment from East Anglia and the increased resuspension due to wind and waves.

Moreover, this schematic highlights the conditions under which one has to be cautious in interpreting sub-surface fluxes from surface data. We find that SPM derived from satellite data can be used to infer SPM concentrations and transport in the East Anglia Plume and Flemish Banks region because the water column is typically well-mixed. However, more information is required in a region like the Rhine ROFI which changes between a well-mixed and stratified state. Hence it is important to have an idea about the state of the plume and the mixing time scales, when trying to infer SPM fluxes from remote

sensing data. In some cases SST images can provide that information, for example, the spring–neap harmonics delineate the Rhine ROFI.

4. Conclusions

In summary, SST and SPM remote sensing images can successfully be used to investigate the intra-annual mesoscale dynamics of the southern North Sea. The monthly composites of SST and SPM delineate the East-Anglia Plume and Rhine ROFI and indicate that intra-annual variability is primarily linked to changing meteorological inputs, in particular, to increasing wind forcing and decreasing surface heating in winter and decreasing wind forcing and increasing surface heating in the summer. In addition rivers supply significant inputs of buoyancy to both coastal boundary layers, which are not in-phase with the solar inputs. Moreover, the harmonic analysis shows the important role played by the tides in the dynamics of the southern North Sea. It also allows us to detect the seasonal front separating well-mixed water in the southern Bight, from the seasonally stratified central North Sea waters. Importantly, the waters of the southern North Sea quickly respond to local meteorological forcing and tidal mixing, in a classic heating-mixing competition near the seasonal front, and a classic freshwater-mixing competition within the ROFIs. Our analysis supports the first order paradigm of Simpson and Hunter (1974) that the water column structure is based on local vertical exchange processes. In the southern North Sea buoyancy inputs from heat and freshwater compete with tidal, wind, wave mixing to establish stratification. Tide, wind and wave mixing also compete with settling and deposition to establish the resulting distribution of fine sediments over the water column. Consequently, vertical mixing also governs the SPM patterns, both directly in terms of the bed shear stresses, and indirectly by modulating the stratification that affects the visibility of SPM in ocean colour imagery.

We conclude that SST and SPM are two complimentary data sets; they respond to the two distinct states of the Rhine ROFI and East Anglia Plume, a well-mixed and a stratified state, in entirely different ways. Moreover, stratification controls the surface visibility of SPM in coastal seas. The Rhine ROFI can switch between stratified and well-mixed states on a typical neap–spring tidal cycle, whereas the downstream region of the East Anglia Plume switches on a seasonal basis. In the Rhine ROFI it is the freshwater inputs and hence the salinity that controls the state of the plume. To the north of the Flamborough and Frisian Fronts, it is the thermal stratification that controls the seasonal vertical stratification. This shows the paramount importance of temporal and spatial variations in tidal and wind mixing in competition with heat and freshwater inputs in controlling the intricate surface signatures of SST and SPM in a shallow shelf sea, as summarised in Fig. 12.

Acknowledgements

The authors thank the SeaWiFS Project (Code 970.2) and the Distributed Active Archive Center (Code 902), the Dundee satellite receiving station, the SeaDAS software team (NASA GSFC) and MUMM for the atmospheric correction extension. The authors are grateful to Loana Arentz, Han Winterwerp, Michel de Nijs, Sharon Tatman, Matthew Turner and Reinold Pasterkamp for assistance with SeaDAS processing. We thank the Dutch ministry of public works Rijkswaterstaat (the Netherlands) for temperature, tide, discharge and solar radiation data, the Royal Dutch Met Office (KNMI, the Netherlands) for wind data and Hans Roozekrans (KNMI) for SST data. We thank The Geological Survey of the Netherlands (TNO) for permission to use their data. Part of the analysis presented in this paper was funded by the EU FP6 project ECOOP. Three anonymous reviewers and the editor are thanked.

References

van Alphen, J.S.L.J., 1990. A mud balance for Belgian–Dutch coastal waters between 1969 and 1986. Netherlands Journal of Sea Research 25, 19–30.

Arentz, L., 2005. Remote sensing of the river Rhine Plume. M.Sc. Thesis, Delft University of Technology, Department of Civil Engineering and Geosciences, the Netherlands. <http://repository.tudelft.nl/view/ir/uuid%3A49f188fb-fade-48b2-b0ec-bdc26caae3cf/>.

Baars, M., Oosterhuis, S., Kuipers, B., 2003. Plume & Bloom: water mass patterns and nutrient dynamics in the central part of the Southern Bight. Annual Report 2002. Royal Netherlands Institute for Sea Research, Texel, pp. 11–13.

de Boer, G.J., Pietrzak, J.D., Winterwerp, J.C., 2006. On the vertical structure of the Rhine region of freshwater influence. Ocean Dynamics 56 (3–4), 198–216.

de Boer, G.J., Pietrzak, J.D., Winterwerp, J.C., 2009. SST observations of upwelling induced by tidal straining in the Rhine ROFI. Continental Shelf Research 29, 263–277.

Booij, N., Ris, R.C., Holthuijsen, L.H., 1999. A third-generation wave model for coastal regions, Part I, Model description and validation. Journal of Geophysical Research C4 (104), 7649–7666.

Brown, J., Hill, A.E., Fernand, L., Horsburg, K.J., 1999. Observations of a seasonal jet-like circulation at the Central North Sea Cold Pool Margin. Estuarine, Coastal and Shelf Science 48, 343–355.

Dronkers, J., Van Alphen, J.S.L.J., Borst, J.C., 1990. Suspended sediment transport processes in the southern North Sea. In: Cheng, R.T. (Ed.), Residual Currents and Long Term Transport. Springer, New York, pp. 302–319.

Dyer, K.R., Moffat, T.J., 1998. Fluxes of suspended matter in the East Anglian Plume southern North Sea. Continental Shelf Research 18, 1311–1331.

Eisma, D., 1981. Supply and deposition of suspended matter in the North Sea. In: Nio, S.-D., Shüttenhelm, R.T.E., Van Weering, Tj.C.E. (Eds.), Holocene Marine Sedimentation in the North Sea Basin. Special Publication Number 5 of the International Association of Sedimentologists. Blackwell Scientific Publishers, Oxford, pp. 415–428.

Eisma, D., 1993. Suspended Matter in the Aquatic Environment. Springer-Verlag, Berlin.

Eisma, D., Kalf, J., 1987. Dispersal, concentration and deposition of suspended matter in the North Sea. Journal of the Geological Society of London 144, 161–178.

Eleveld, M.A., Pasterkamp, R., van der Woerd, H.J., 2004. A survey of total suspended matter in the southern North Sea based on the 2001 SeaWiFS data. EARSeL eProceedings 3 (2), 166–178. Online available at URL: http://www.eproceedings.org/.

Eleveld, M.A., Pasterkamp, R., van der Woerd, H.J., Pietrzak, J., 2006. Suspended particulate matter from SeaWiFS data: statistical validation, and verification against the physical oceanography of the southern North Sea. Ocean Optics OOXVIII, 9–14 October 2006, Montreal. Lewis Conference Services International Inc., Halifax (CA), 60234, p. 18.

Eleveld, M.A., Pasterkamp, R., van der Woerd, H.J., Pietrzak, J.D., 2008. Remotely sensed seasonality in the spatial distribution of sea-surface suspended particulate matter in the southern North Sea. Estuarine, Coastal and Shelf Science 80 (1), 103–113. doi:10.1016/j.ecss.2008.07.015.

Fettweis, M., Van den Eynde, D., 2003. The mud deposits and the high turbidity in the Belgian–Dutch coastal zone, Southern Bight of the North Sea. Continental Shelf Research 23 (7), 669–691.

Gerritsen, H., Vos, R.J., van der Kaaij, T., Lane, A., Boon, J.G., 2000. Suspended sediment modelling in a shelf sea (North Sea). Coastal Engineering 41, 317–352. Gerritsen, H., Boon, J.G., van der Kaaij, T., Vos, R.J., 2001. Integrated modelling of suspended matter in the North Sea. Estuarine, Coastal and Shelf Science 53, 581–594.

Geyer, W.R., 1993. The importance of suppression of turbulence by stratification on the estuarine turbidity maximum. Estuaries 16 (1), 113–125.

Hill, A.E, James, I.D., Linden, P.F., Mathews, J.P., Prandle, D., Simpson, J.H., Gmitrowicz, E.M., Smeed, D.A., Lwiza, K.M.M., Durazo, R., Fox, A.D., Bowers, D.G., Weydert, M., 1993. Dynamics of tidal mixing fronts in the North Sea. Philosophical Transactions: Physical Sciences and Engineering. Understanding the North Sea System, 431–446.

Hill, A.E., Brown, J., Fernand, L., Holt, J., Horsburgh, K.J., Proctor, R., Raine, R., Turrell, W.R., 2008. Thermohaline circulation of shallow tidal seas. Geophysical Research Letters 35, L11605. doi:10.1029/2008GL033459.

Holligan, P.M., Aarup, T., Groom, S.B., 1989. The North Sea: satellite colour atlas. Continental Shelf Research 9, 667–765.

Holt, J.T., James, I.D., 1999. A simulation of the southern North Sea in comparison with measurements from the North Sea Project, Part 2: Suspended particulate matter. Continental Shelf Research 19, 1617–1642.

Irion, G., Zöllmer, 1998. Clay mineral associations in fine-grained surface sediments of the North Sea. Journal of Sea Research 41, 119–128.

Joordens, J.C.A., Souza, A.J., Visser, A., 2001. The influence of tidal straining and wind on suspended matter and phytoplankton distribution in the Rhine outflow region. Continental Shelf Research 21, 301–325.

de Kok, J.M., de Valk, C., van Kester, J.H.Th.M., de Goede, E., Uittenbogaard, R.E., 2001. Salinity and temperature stratification in the Rhine Plume. Estuarine, Coastal and Shelf Science 53, 467–475.

Lacroix, G., Ruddick, K., Ozer, J., Lancelot, C., 2004. Modelling the impact of the Scheldt and Rhine/Meuse plumes on the salinity distribution in Belgian waters (southern North Sea). Journal of Sea Research 52, 149–163.

Lafite, R., Shimwell, S., Grochowski, N., Dupont, J.P., Nash, L., Salomon, J.C., Cabioch, L., Collins, M., Gao, S., 2000. Suspended particulate matter fluxes through the Straits of Dover, English Channel: observations and modelling. Oceanologica Acta 23 (6), 687–700.

Lee, A.J., 1980. North Sea: physical oceanography. In: Banner, F.T., Collins, M.B., Massie, K.S. (Eds.), The North-West European Shelf Seas: The Seabed and the Sea in Motion. 2. Physical and Chemical Oceanography, and Physical Resources. Elsevier Oceanography Series, 24B. Elsevier, Amsterdam, pp. 467–493.

McCandliss, R.R., Jones, S.E, Hearn, M., Latter, R., Jago, C.F., 2002. Dynamics of suspended particles in coastal waters (southern North Sea) during a spring bloom. Journal of Sea Research 47, 285–302.

McCave, I.N., 1987. Fine sediment sources and sinks around the East Anglian Coast. Journal of the Geological Society of London 144, 149–152.

Morel, A., Prieur, L., 1977. Analysis of variations in ocean color. Limnology and Oceanography 22 (4), 709–722.

Morel, A., Gentili, B., 1996. Diffuse reflectance of oceanic waters. III. Implication of bidirectionality for the remote-sensing problem. Applied Optics 35 (24), 4850–4862.

Nihoul, J.C.J., Hecq, J.H., 1984. Influence of the residual circulation on the physicochemical characteristics of water masses and the dynamics of ecosystems in the Belgian coastal zone. Continental Shelf Research 3, 167–174.

de Nijs, M.A.J., Winterwerp, J.C., Pietrzak, J.D., 2010. The effects of internal flow structure on SPM entrapment in the Rotterdam. Journal of Physical Oceanography 40, 2357–2380.

de Nijs, M.A.J, Pietrzak, J.D., Winterwerp, J.C., 2011. Advection of the salt wedge and evolution of the internal flow structure in the Rotterdam Waterway. Journal of Physical Oceanography (in press).

North Sea Task Force, 1993. North Sea Quality Status Report 1993. Oslo and Paris Commissions, London. Olsen and Olsen, Fredensborg, Denmark.

Otto, L., 1966. Light attenuation in the North Sea and the Dutch Waddden Sea in relation to secchi disc visibility and suspended matter. Netherlands Journal of Sea Research 3, 28–51.

Otto, L., 1967. Investigations on optical properties and water masses of the Southern North Sea. Netherlands Journal of Sea Research 3, 532–551.

Otto, L., Zimmerman, J.T.F., Furnes, G.K., Mork, M., Sætre, R., Becker, G., 1990. Review of the physical oceanography of the North Sea. Netherlands Journal of Sea Research 26, 161–238.

Pasterkamp, R., van Drunen, M., 2002. Noordzee-atlas voor zwevend stof op basis van satellietbeelden in 2000 (atlas of suspended sediment transport for the North Sea: based on satellite imagery of 2000). Technical Report RIKZ/IT/2002.102. National Institute for Coastal and Marine Management/RIKZ.

Pasterkamp, R., Eleveld, M., van der Woerd, H., van Drunen, M., 2003. Noordzeeatlas voor zwevend stof op basis van satellietbeelden in 2001. Report AGI-GAR-2003-38, Rijkswaterstaat—Adviesdienst Geo-informatie en ICT, Delft.

Pasterkamp, R., Eleveld, M.A., van der Woerd, H., 2005. Design of single-band sediment algorithms: wavelength considerations. In: Proceedings of the 8th Conference on Remote Sensing for Marine and Coastal Environments, 17–19 May 2005, Halifax, Canada. Altarum Institute (formerly ERIM), Ann Arbor, Michigan.

Pingree, R.D., Griffiths, D.K., 1978. Tidal fronts on the shelf seas around the British Isles. Journal of Geophysical Research 83, 4615–4622.

Pleskachevsky, A., Gayer, G., Horstmann, J., Rosenthal, W., 2005. Synergy of satellite remote sensing and numerical modeling for monitoring of suspended particulate matter. Ocean Dynamics 55 (1), 2–10.

Postma, H., 1961. Suspended matter and sechi disc visibility in coastal waters. Netherlands Journal of Sea Research 1, 359–390.

Prandle, D., 1978. Residual flows and elevations in the Southern North Sea. Proceedings of the Royal Society of London A 259, 189–228.

Prandle, D., Loch, S.G., Player, R.J., 1993. Tidal flow through the Straits of Dover. Journal of Physical Oceanography 23 (1), 23–37.

van Raaphorst, W., Philippart, C.J.M., Smit, J.P.C., Dijkstra, F.J., Malschaert, J.F.P., 1998. Distribution of suspended particulate matter in the North Sea as inferred from NOAA/AVHRR reflectance images and in situ observations. Journal of Sea Research 39, 197–215.

Roelvink, J.A., Van der Kaaij, T., Ruessink, G., 2001. Calibration and verification of large-scale 2D/3D flow models phase 1. Sub-product 2, MARE Report, Reference Z3029.11. WL|Delft Hydraulics, Delft.

Roozekrans, J.N., Prangsma, G.J. 1992. Observatie van het aardatmosfeer systeem door de NOAA-satellieten (ontvangst, productie, toepassing en gebruik van de NOAA-data. Tech. rept. BCRS report 92-02. BCRS Projects IS-3.5 and OP-1.12, Dutch.

Ruddick, K.G., Ovidio, F., Rijkeboer, M., 2000. Atmospheric correction of SeaWIFS imagery for turbid coastal and inland waters. Applied Optics 39 (6), 897–912.

de Ruijter, W.P.M., van der Giessen, A., Groenendijk, F.C., 1992. Current and density structure in the Netherlands coastal zone. In: Prandle, D. (Ed.), Coastal and Estuarine Studies, Vol 40: Dynamics and exchanges in estuaries and the coastal zone. AGU, Washington, USA.

Saunders, R.W., Kriebe, K.T., 1988. An improved method for detecting clear sky and cloudy radiances from AVHRR data. International Journal of Remote Sensing 9, 123–150.

Simpson, J.H., Hunter, J.R., 1974. Fronts in the Irish Sea. Nature 250, 404–406. Simpson, J.H., Bos, W.G., Schirmer, F., Souza, A.J., Rippeth, T.P., Jones, S.E., Hydes, D., 1993. Periodic stratification in the Rhine ROFI in the North Sea. Oceanologica Acta 16 (1), 23–32.

Simpson, J.H., 1998. Tidal processes in Shelf Seas. In: Brink, K., Robinson, A. (Eds.), The SEA, The Global Coastal Ocean, vol. 10. John Wiley, pp. 113–150.

Souza, A.J., Simpson, J.H., 1997. Controls on stratification in the Rhine ROFI system. Journal of Marine Systems 12, 311–323.

Souza, A., Holt, J., Proctor, R., 2007. Modelling SPM on the NW European Shelf Seas. In: Balson, P.S., Collins, M.B. (Eds.), Coastal and Shelf Sediment Transport, 274. Geological Society of London, Special Publications, pp. 147–158.

Stelling, G.S., Van Kester, J.A.Th.M., 1994. On the approximation of horizontal gradients in sigma co-ordinates for bathymetry with steep bottom slopes. International Journal for Numerical Methods in Fluids 18 (18), 915–935.

Suijlen, J.M., Duin, R.N.M., 2001. Variability of near-surface total suspended-matter concentrations in the Dutch coastal zone of the North Sea: Climatological study on the suspended matter concentrations in the North Sea. Report RIKZ/OS/2001.150X. RIKZ, The Hague.

Suijlen, J.M., Duin, R.N.M., 2002. Atlas of near-surface total suspended matter concentrations in the Dutch coastal zone of the North Sea. Tech. Report RIKZ/2002.059. National Institute for Coastal and Marine Management/RIKZ, the Hague, the Netherlands.

von Storch, H., Zwiers, F.W., 1999. Statistical Analysis in Climate Research. Cambridge University Press.

Swart, D.H., 1974. Offshore sediment transport and equilibrium beach profiles. Ph.D. Thesis Delft Univ. Technol./Delft Hydraulics Laboratory Publ. No. 131, Delft.

Visser, M.P., 1970. The turbidity of the Southern North Sea. Deutsche Hydrographische Zeitschrift 23, 97–117.

Visser, A.W., Souza, A.S., Hessner, K., Simpson, J.H., 1994. The effect of stratification on tidal current profiles in a region of freshwater influence. Oceanologica Acta 17 (4), 369–381.

Visser, M., de Ruijter, W.P.M., Postma, L., 1991. The distribution of suspended matter in the Dutch coastal zone. Netherlands Journal of Sea Research 27, 127–143.

Wild-Allen, K., Lane, A., Tett, P., 2002. Phytoplankton, sediment and optical observations in Netherlands coastal water in spring. Journal of Sea Research 47, 303–315.

van der Woerd, H., Pasterkamp, R., 2004. Mapping of the North Sea turbid coastal waters using SeaWiFS data. Canadian Journal of Remote Sensing 30 (1), 44–53.

Figures

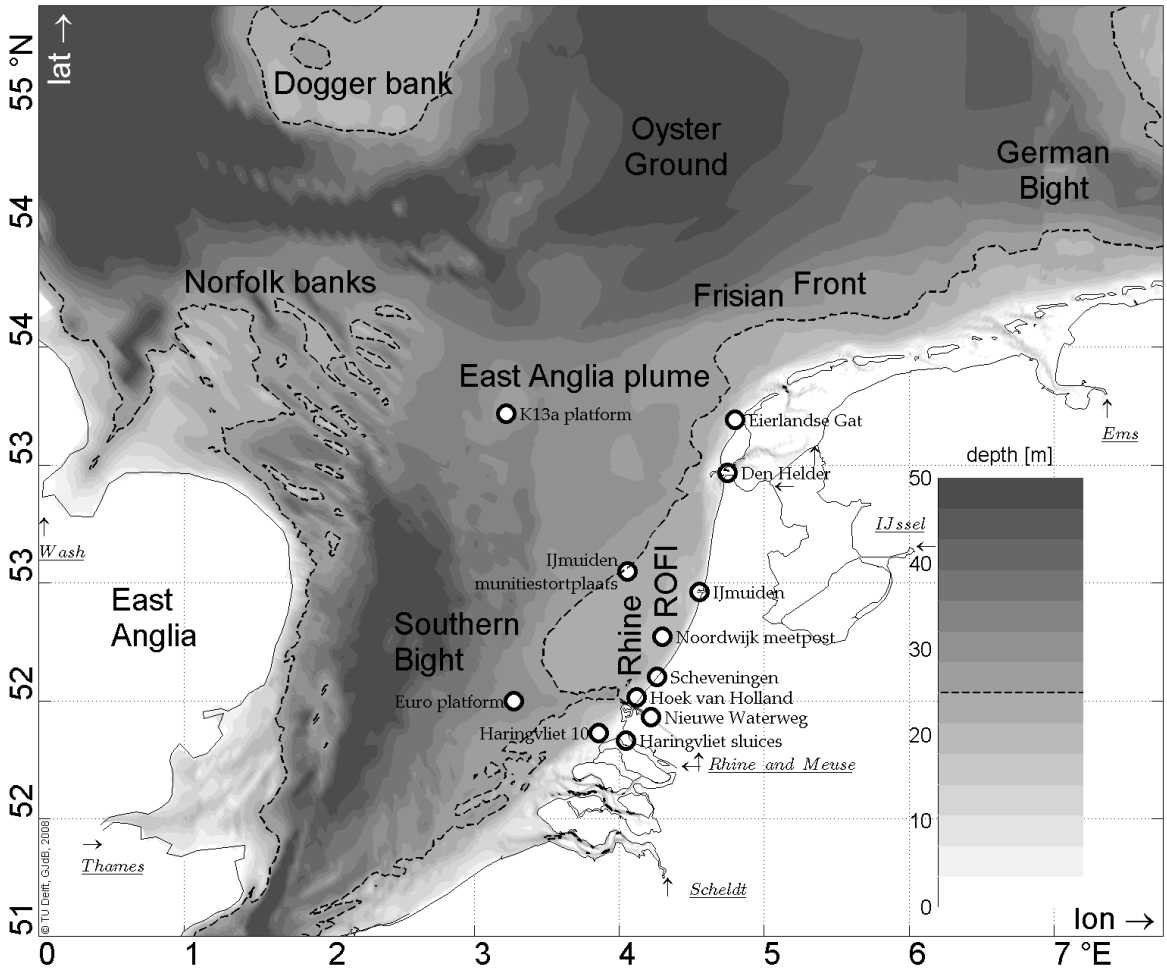

Fig. 1. The bathymetry of the central and southern North Sea and the English Channel. The area to the south of Dogger Bank is referred to here as the southern North Sea. The location of the meteorological and oceanographic stations is shown. The Rhine ROFI is formed by the discharge of water from the Rhine–Meuse–Scheldt River system through the Rotterdam Waterway, Haringvliet Sluices and Western Scheldt.

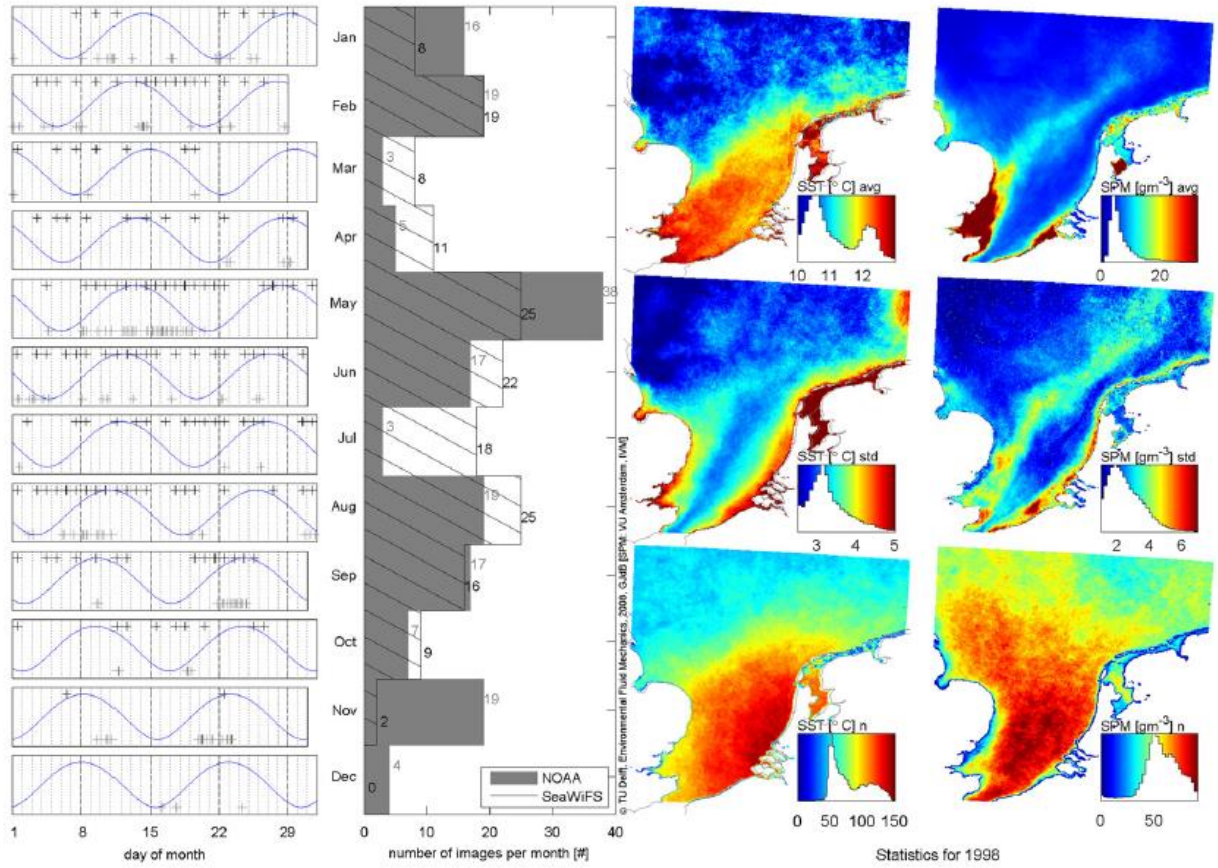

Fig. 2. The left-hand side shows the temporal distribution of the SST and SPM images (the lower and upper + signs, respectively) and their relationship to the spring–neap tidal cycle (the blue curve, a peak corresponds to spring and a trough to neap tide). The middle panel shows the number of images available per month. The right-hand side panel shows distribution of the annual mean (top), standard deviation (middle) and total number of unclouded pixels (bottom) for 1998. The insets are the colour bars. The white areas in the colour bars are the histograms of the pixels values, where the x-axis corresponds to the pixels value (SST or SPM) and the y-axis corresponds to the relative frequency distribution of the pixel values.

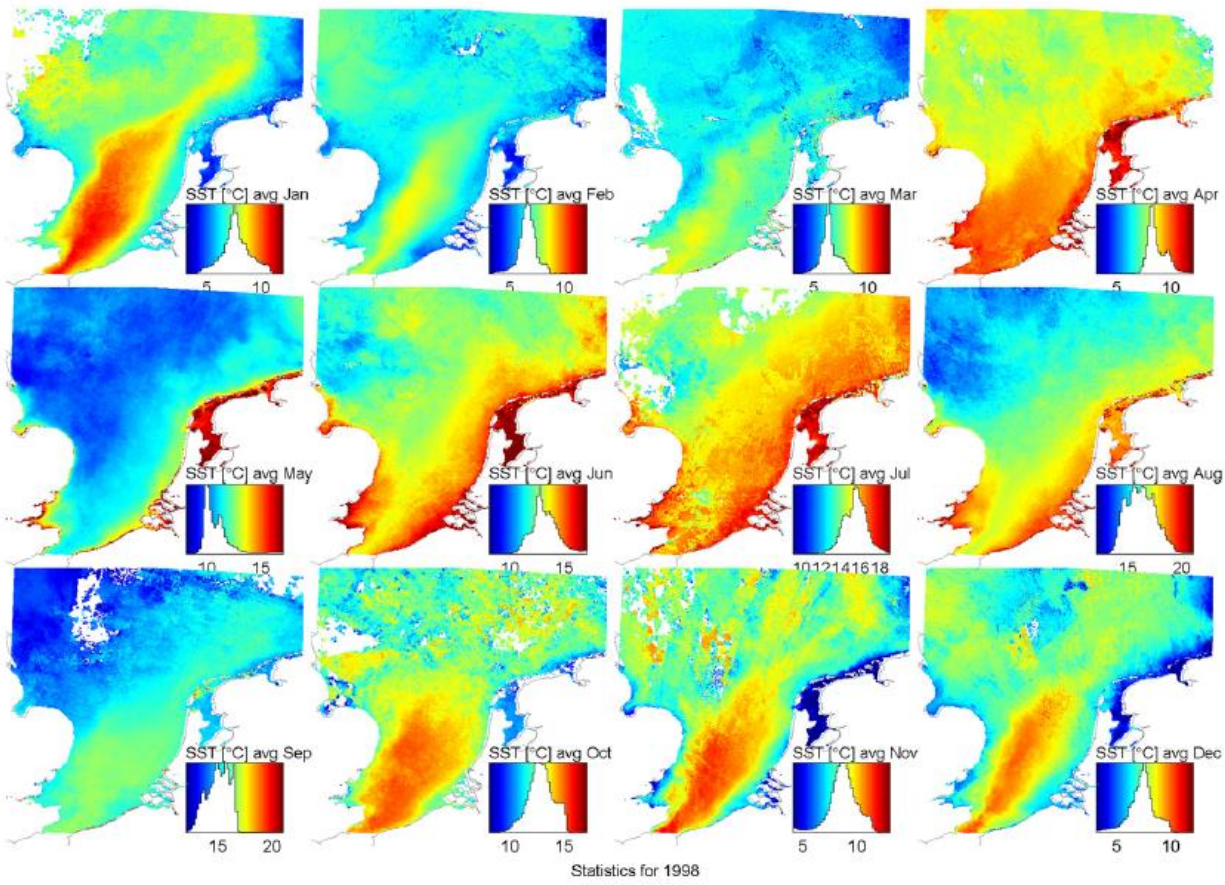

Fig. 3. Plan views of the monthly mean values of SST. The insets are the colour bars, note that they differ per month. The white areas in the colour bars are the histograms of the pixels values, where the x-axis corresponds to the SST pixel value and the y-axis corresponds to the relative frequency distribution of the pixel values. The distinct seasonal cycle is evident, with a band of colder waters being visible in the continental and English coastal waters during the winter months and warmer coastal waters in the summer.

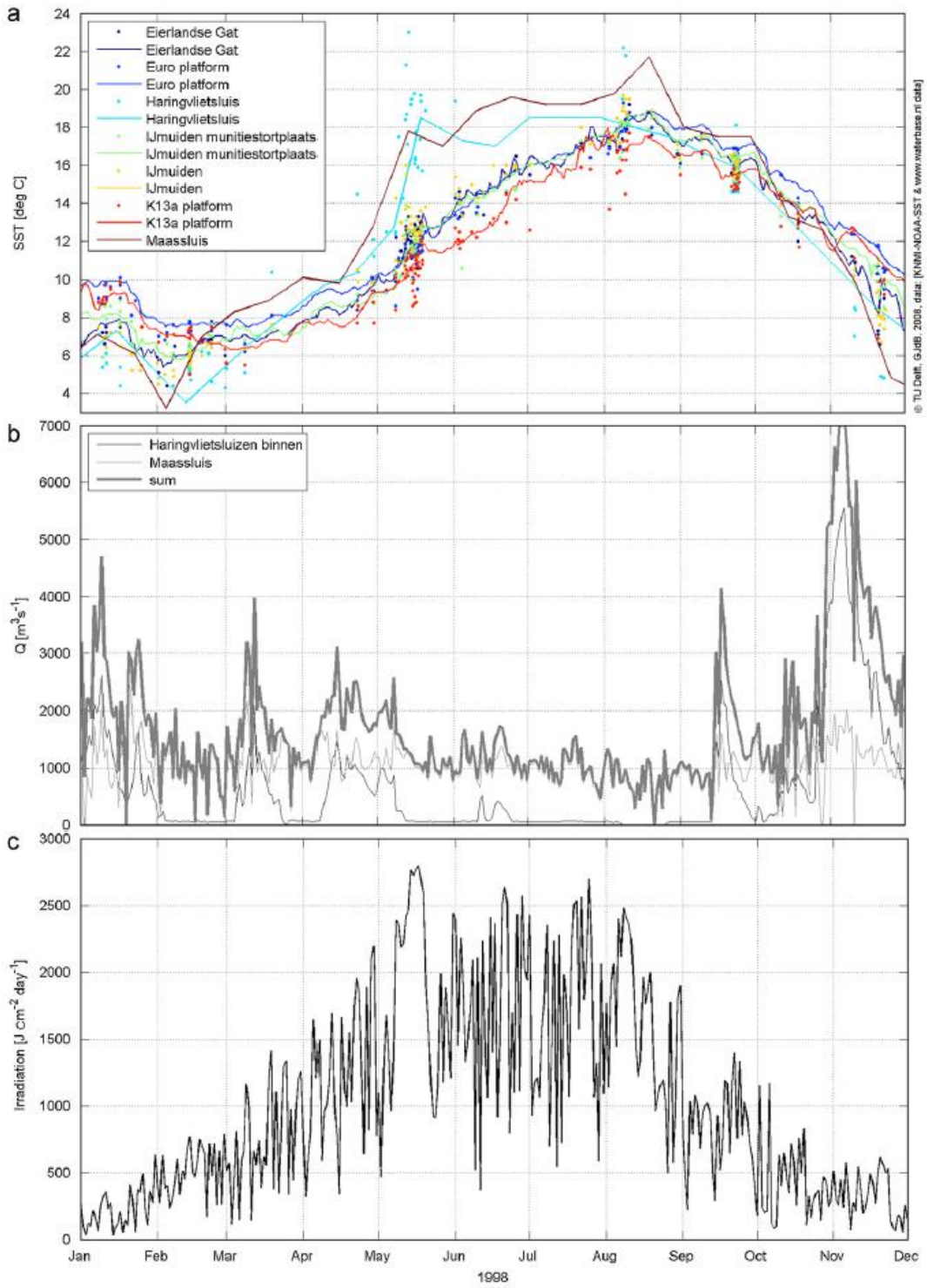

Fig. 4. The oceanographic and meteorological conditions during 1998. (a) (Top panel) The temperature recorded at 1 m below the surface at a number of stations. The dots show the available values recorded by the NOAA satellite images at the same locations. (b) (Centre panel) The river discharge during 1998. The Rhine–Meuse discharge is regulated. If the discharge is less than 1700 m^3 s^{-1} then all of the discharge is through the Rotterdam Waterway. If greater than 1700 m^3 s^{-1} then the Haringvliet sluices are opened at LW. Between 1700 and 3900 m^3 s^{-1} the fresh water discharge in the Rotterdam Waterway is regulated to be 1500 m^3 s^{-1}. The mean annual river discharge during 1998 was 1750 m^3 s^{-1}. (c) (Bottom panel) The seasonal cycle of irradiation. Source: Rijkswaterstaat (a,b) and KNMI (c)

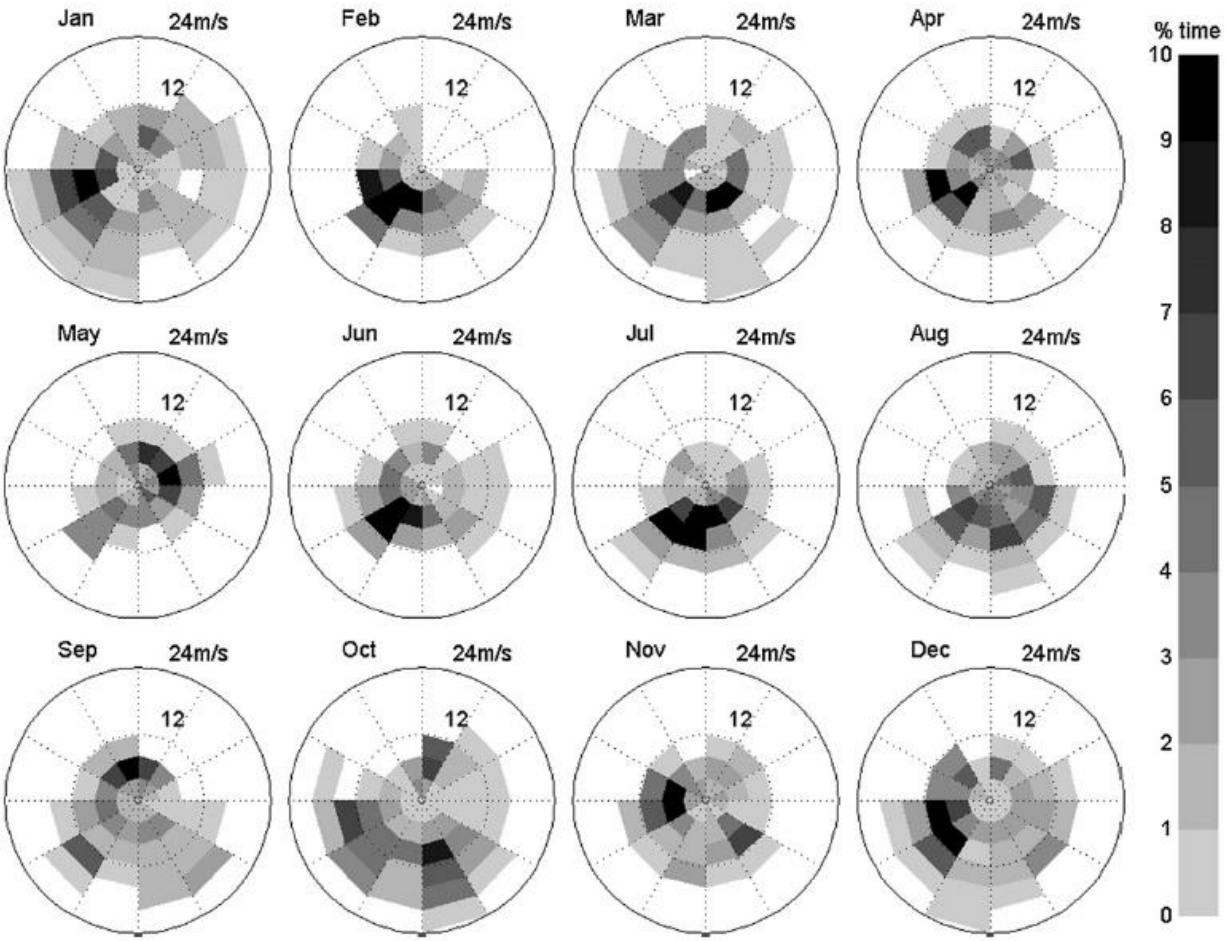

Fig. 5. Wind roses showing the distribution of the monthly wind speeds and directions. The wind data were recorded at 10 m height at the station ″Meetpost Noordwijk″. The magnitude is the greatest in the winter months. While SW winds dominate the annual wind record, there is considerable variability in the winds. Source: KNMI

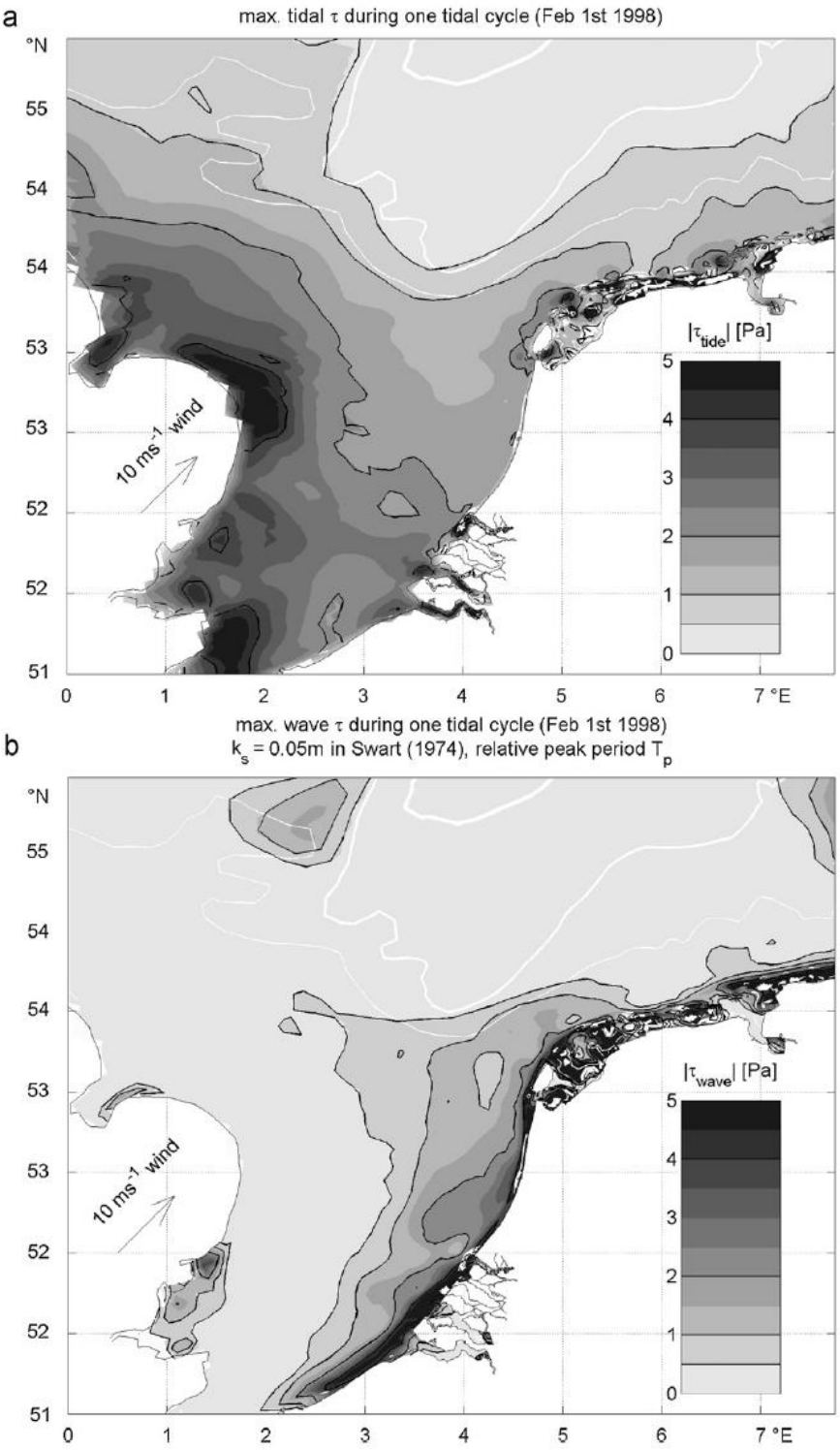

Fig. 6. Maximum bed shear stresses [Pa] computed during one semi-diurnal tidal cycle on February 1, 1998 from (a) a simulation with a 10-layer barotropic tidal model set-up of Delft3D-FLOW and (b) a run that employed a two-way coupling with an hourly SWAN wave simulation with a constant SW wind of 10 m s^{-1}. The white contours depict values of the Simpson–Hunter criterion h/u^3 using the same definition of the stratification parameter S as in Pingree and Griffiths (1978): $S=\log_{10}(h/C_d u^3 10^4)$) where C_d is 0.0025 and the factor 10^4 is included to convert cfs units. The thin, medium and thick lines depict values of S=1, 1.5 and 2, respectively. S=1 indicates areas that are well-mixed, S=1.5 indicates transitional areas and S=2 seasonally stratified regions.

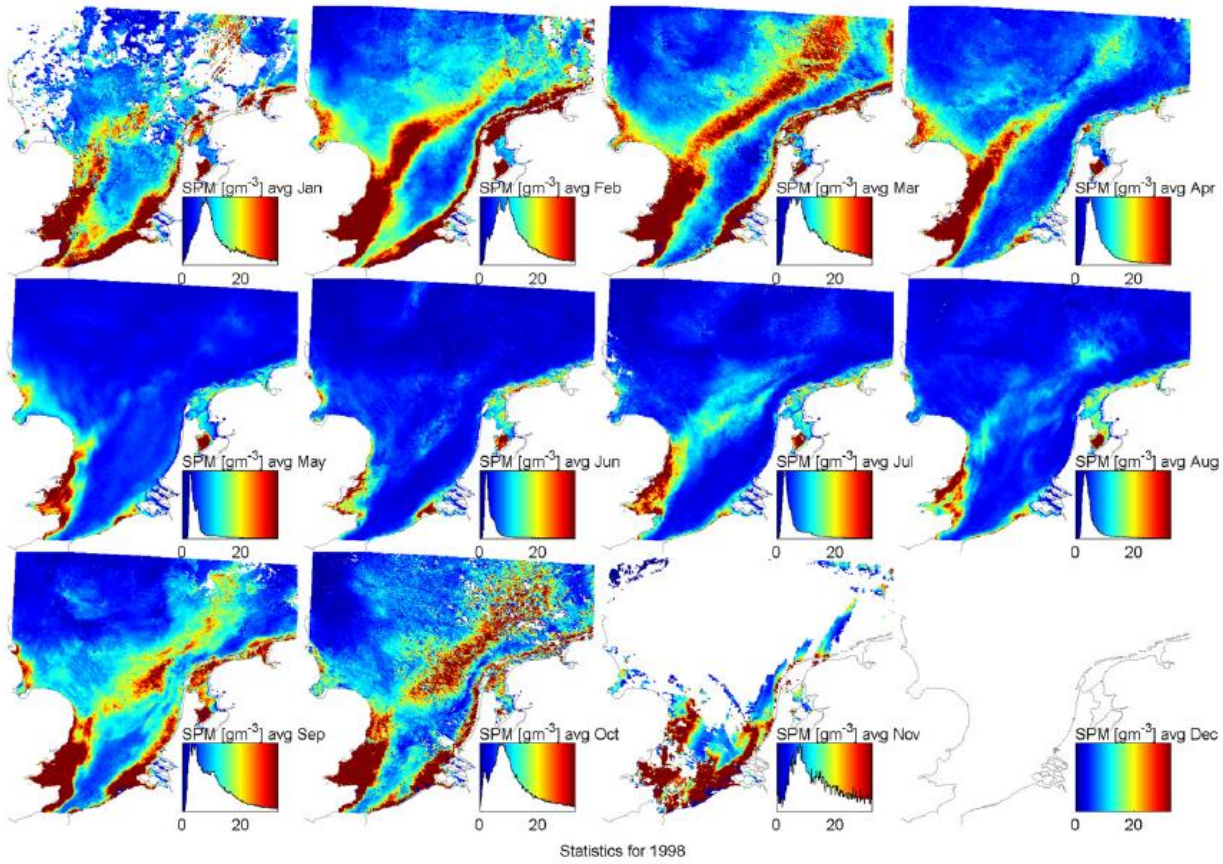

Fig. 7. Plan views of the monthly averages of near-surface SPM. The insets are the colour bars, note that they are identical for all months. The white areas in the colour bars are the histograms of the pixels values, where the *x*-axis corresponds to the SPM pixel value and the *y*-axis corresponds to the relative frequency distribution of the pixel values. Note the large values of SPM during the winter in the Belgium, Dutch, German and UK coastal waters, particularly at the locations of the Rhine ROFI, the East Anglia Plume and Frisian Front. Minimal SPM values are observed along the Dutch coastal zone from April to August. Towards the end of the summer almost all surface SPM in the Dutch coastal zone has vanished.

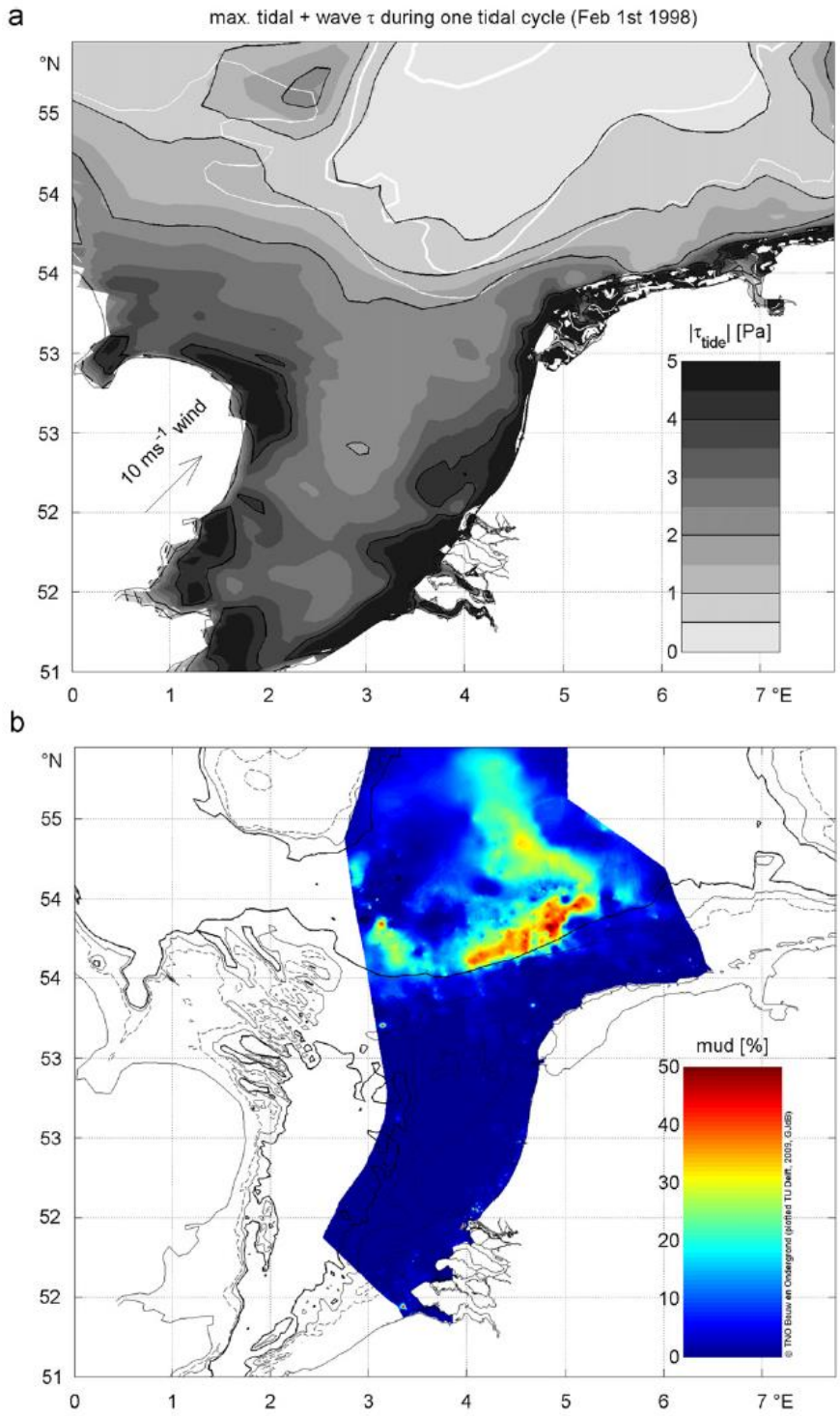

Fig. 8. (a) Maximum bed shear stresses [Pa] computed during one semi-diurnal tidal cycle on February 1, 1998 from the combined tide and wave stresses for a constant SW wind of 10 m s^{-1}. The white contours depict values of the Simpson–Hunter criterion. The thin, medium and thick lines depict values of S=1, 1.5 and 2, respectively. S=1 indicates areas that are well-mixed, S=1.5 indicates transitional areas and S=2 seasonally stratified regions and (b) the distribution of mud in the upper sediment layer of the bed from box cores taken in the Dutch sector of the southern North Sea. The data were provided courtesy of The Geological Survey of the Netherlands (TNO). The black lines indicate bathymetric contours. The thin dashed, thin and thick lines indicate depths of 25, 30 and 35 m, respectively.

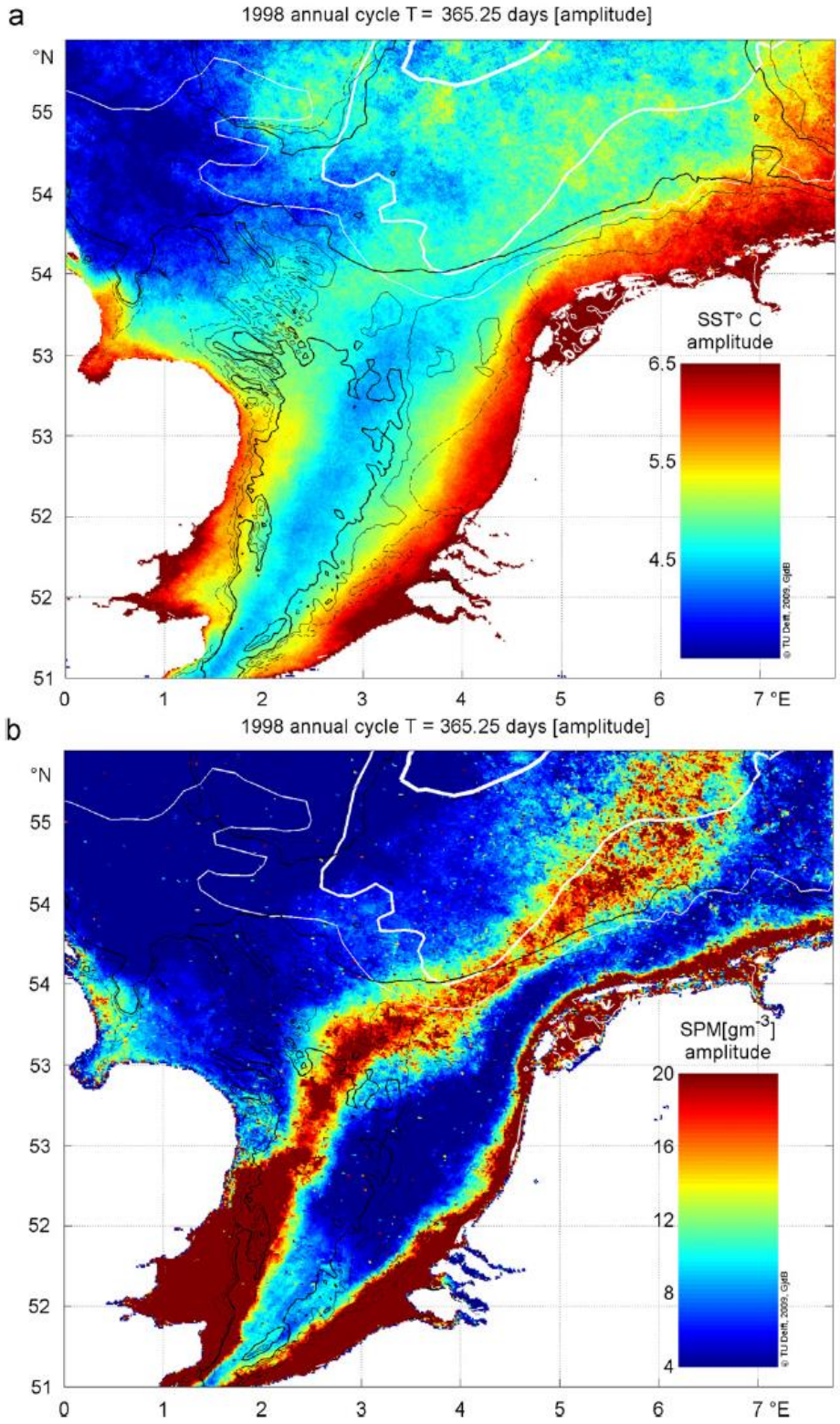

Fig. 9. The spatial distribution of the amplitude of the annual harmonic fitted with Eq. (1) for A1 (x,y) of (a) SST and (b) SPM using the 1998 data. The white contours depict values of the Simpson–Hunter criterion. The thin, medium and thick lines depict values of S=1, 1.5 and 2, respectively. S=1 indicates areas that are well-mixed. The black lines indicate bathymetric contours. The thin dashed, thin and thick lines indicate depths of 25, 30 and 35 m, respectively.

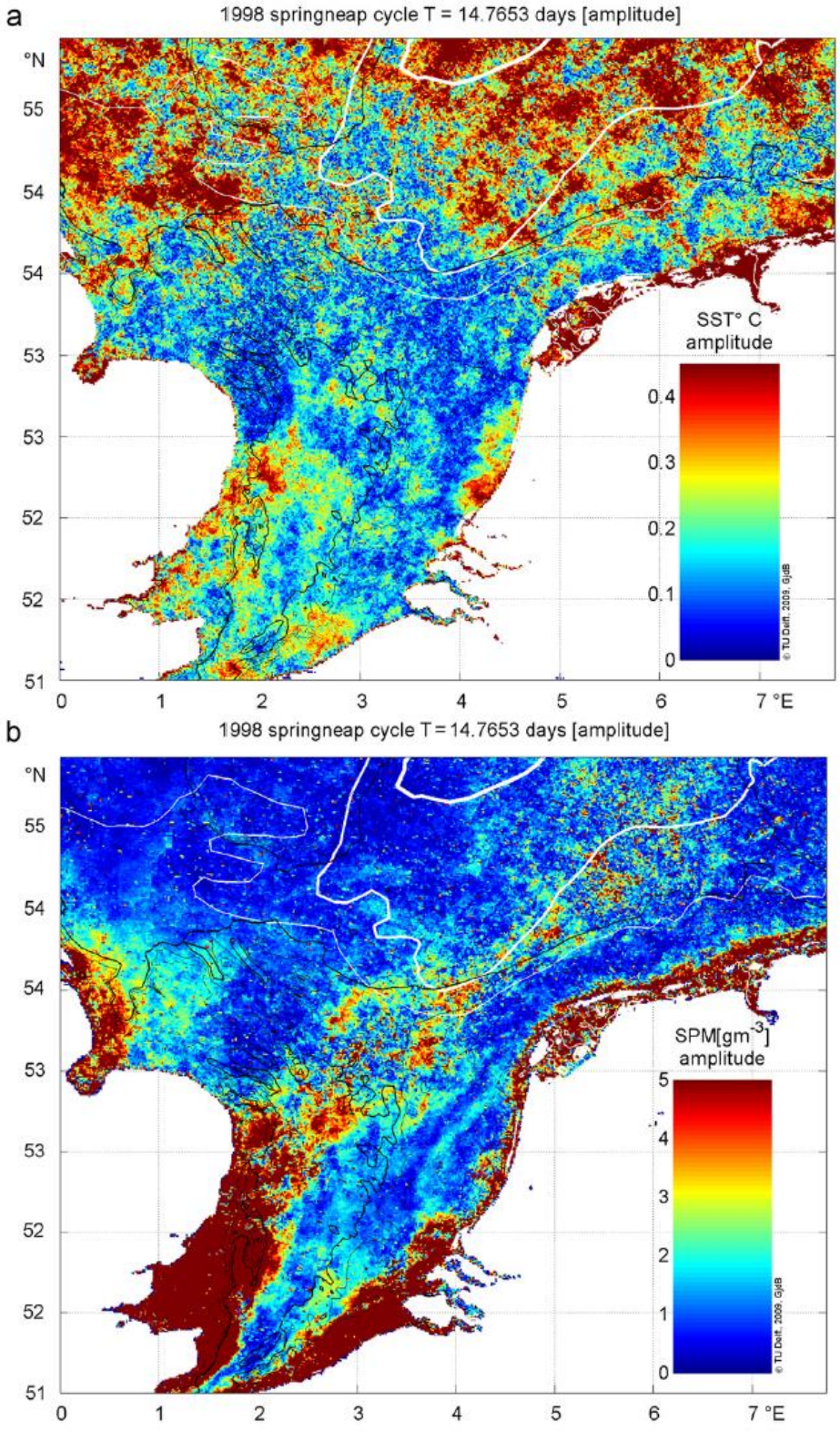

Fig. 10. The spatial distribution of the amplitude of the spring–neap harmonic fitted with Eq. 1 for A2 (x,y) of a) SST and b) SPM using the 1998 data.

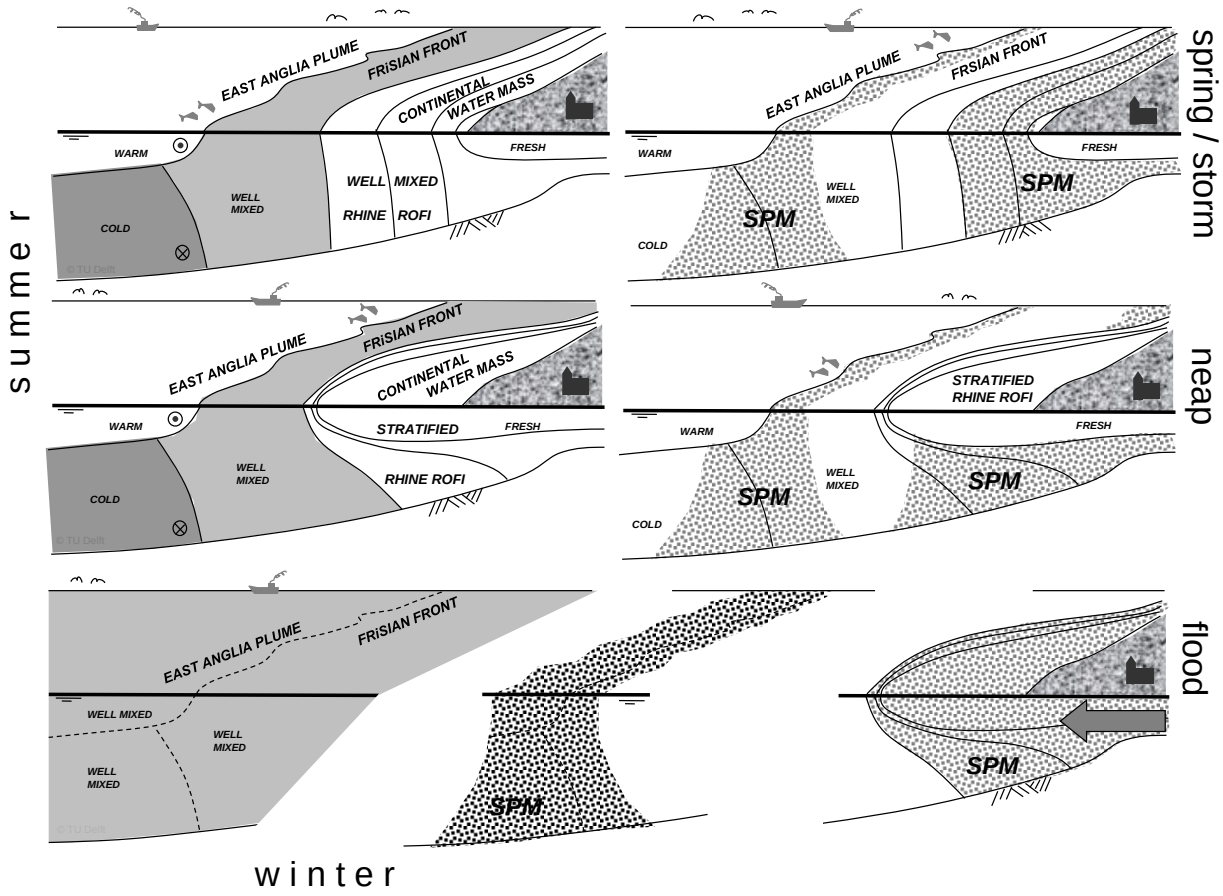

Fig. 11. Schematic showing the visibility of SPM at the surface of the southern North Sea in relation to stratification, redrawn after Simpson et al. (1993) to include the distribution of SPM. On the left, the stratified and well-mixed states of the Rhine ROFI are shown, as well as the region of the seasonal thermocline. On the right, the corresponding SPM distributions are sketched. See Section 3.5 for details.

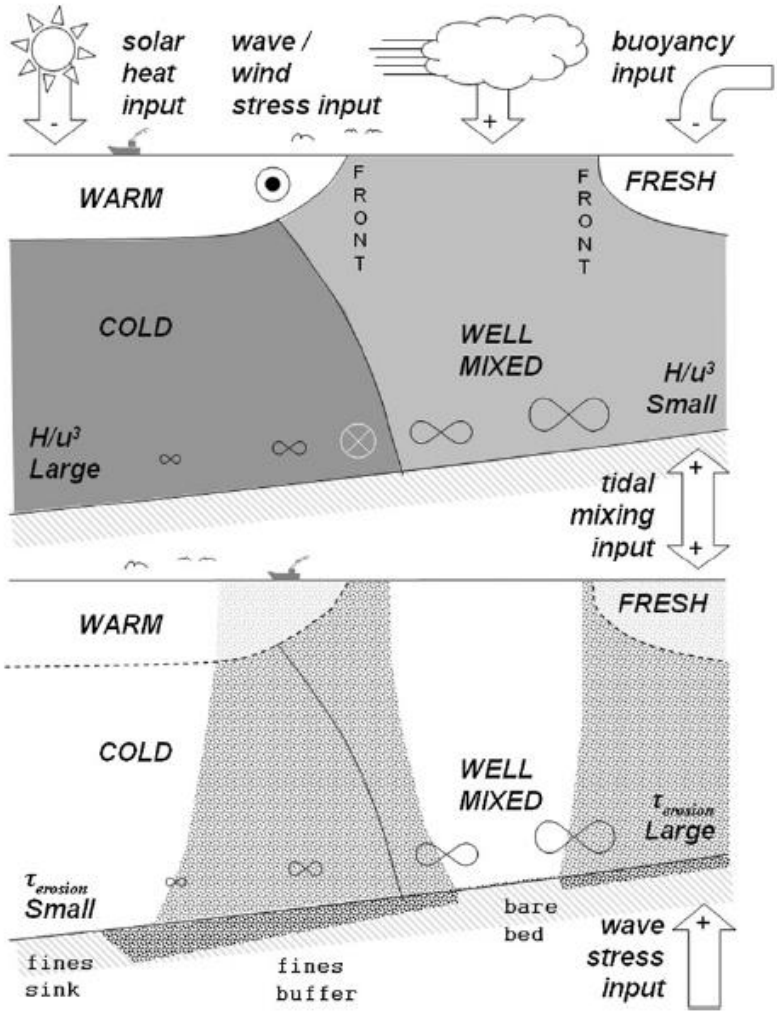

Fig. 12. Schematic summarising the heating-mixing and freshwater-mixing competition in the southern North Sea and the resulting distribution of SPM over the water column and at the bed, after Simpson (1998).